

RESEARCH

Open Access



# Magnetic and gravity modeling and subsurface structure of two geothermal fields in the UAE

Hakim Saibi<sup>1\*</sup> , Mohamed Amrouche<sup>2</sup>, Joseph Batir<sup>3</sup>, Amir Gabr<sup>1</sup> and Abdel-Rahman Fowler<sup>1</sup>

\*Correspondence:  
hakim.saibi@uaeu.ac.ae

<sup>1</sup> Geosciences Department,  
College of Science, United Arab  
Emirates University, Al-Ain, UAE

<sup>2</sup> Schlumberger, Tokyo, Japan

<sup>3</sup> Geothermal Laboratory,  
Southern Methodist University,  
Dallas, USA

## Abstract

There are two low-enthalpy geothermal systems along the eastern border of the United Arab Emirates: Ain Khatt (Khatt City, Ras Al Khaimah Emirate) and Green Mubazzarah–Ain Faidha (GMAF) (Al-Ain City, Abu Dhabi Emirate). The hot springs are likely to be meteoric waters fed through deep-seated faults that intersect the geothermal reservoirs at 2.6–3.8 km depth. Gravity and magnetic data were analyzed by gradient (horizontal derivative “HD”, and improved normalized horizontal tilt angle “INH”), and separately 3D modeled to image the subsurface structure of the two UAE geothermal systems. Bouguer anomalies in GMAF and Ain Khatt range from – 14.2 to 8.09 mGal and – 169.3 to – 122.2 mGal, respectively. Magnetic intensities in GMAF and Ain Khatt vary from 39,327 to 44,718 nT and 43,650 to 44,653 nT, respectively. The UAE hot springs (GMAF and Ain Khatt) are located in mainly high HD and INH regions, which reflect significant discontinuities in the basement rock, such as faults or lithological contacts. A joint inversion of magnetic and gravity data, through Artificial Neural Network (ANN) modeling, was performed to explore and interpret the 3D density and magnetic susceptibility variations. Results show that the hot springs in both geothermal systems are associated with intersecting geological contacts and fault zones. The Green-Mubazzarah–Ain Faidha hot springs may be connected at depth.

## Highlights

- Faults are conduit-like for geothermal fields.
- Flow paths of rising hot waters are mapped.
- Hot springs are structurally controlled.

**Keywords:** Gravity, Magnetic, 3D inversion, Artificial Neural Network, Structure, Modeling, Geothermal, UAE

## Introduction

The United Arab Emirates (UAE) is located at the eastern end of the Arabian Peninsula. Water sources in the UAE are mainly groundwater, including sediment aquifers and fractured bedrock aquifers. Some groundwater sources are geothermal especially those associated with deep fracture systems (Saibi et al. 2021b). These hot springs occurrences are found in several places in the Emirates including Abu Dhabi (The Green Mubazzarah–Ain Faidha) and Ras Al Khaimah Emirate (Ain Khatt) (Saibi et al. 2021c, 2021d). In the Abu Dhabi Emirate, just south of the city of Al Ain lies a limestone mount known as Mount (Jabal) Hafit. The Hafit mountain is a tourist attraction for its scenery and hot springs occurrences, especially in the locality of Green Mubazzarah. The geothermal manifestations at Green Mubazzarah are located in the foothills of Mount Hafit. Hafit mountain is the dominant bedrock exposure in the Al Ain region, and is divided by the UAE–Oman international border. The Green Mubazzarah hot springs flow into small streams to form a warm lake. The main utilization of these thermal springs is for recreational bathing and fish farming. The previous geophysical studies of the Al Ain area are regional and focused on the study of the structural evolution of Mount Hafit (Ali et al. 2009; Woodward 1994; El-Mahmoudi and Gabr 2006; Saibi et al., 2017, 2019a, b, 2021d; Saibi, 2018).

Saibi et al. (2021d) performed a magnetotelluric survey which discovered a geothermal reservoir beneath Green Mubazzarah (Al-Ain) in Mesozoic basement and overlying Tertiary carbonates with depths ranging from 1 to 4 km. This study confirms the existence of E–W striking steeply dipping normal faults that may connect Green Mubazzarah and the Ain Faidha hot springs. Saibi (2018), Saibi et al. 2019b) developed 3D magnetic models at UAE geothermal fields and revealed structure control on hot water flow patterns.

Potential fields (gravity and magnetic) are non-destructive geophysical methods which help to delineate and investigate the subsurface structures such as basement rocks, faults/contacts and geological features (intrusions, dykes). The cost efficiency and simplicity of acquisition for potential fields methods make them highly affordable and practical, and their application has proved successful in solving geotechnical challenges (Butler 1984; Pringle et al. 2012), structural interpretations (Searle and Ali 2009; Saibi et al. 2019a, b) and other geothermal investigations (Hunt et al. 2009; Abdel Zaher et al. 2018a, b; Bilim et al. 2017; Gailler et al. 2014).

The aim of this study is to complement the previous works on the geothermal activity in the UAE and delineate the subsurface structures of these geothermal fields, in order to identify the 3D-geometry of the hot springs systems. Here, we present the results of magnetic and gravity acquired data, and apply corrections to the observed potential field data, after which we apply the potential field data derivative (horizontal derivative and improved normalized horizontal tilt angle). 3D inversion and Artificial Neural Network (ANN) methods were applied to the potential field data in order to retrieve the 3D distribution of the density and magnetic susceptibility for the studied areas, and correlate the similarities between the gravity and the magnetic results. The results of this paper help to highlight the subsurface structure of two geothermal areas: (1) the Green Mubazzarah–Ain Faidha (GMAF) hot springs, located near Al-Ain city, Abu Dhabi Emirate, and (2) the Ain Khatt (AK) hot springs, located in Khatt village, Ras Al Khaimah (RAK) Emirate (Fig. 1).

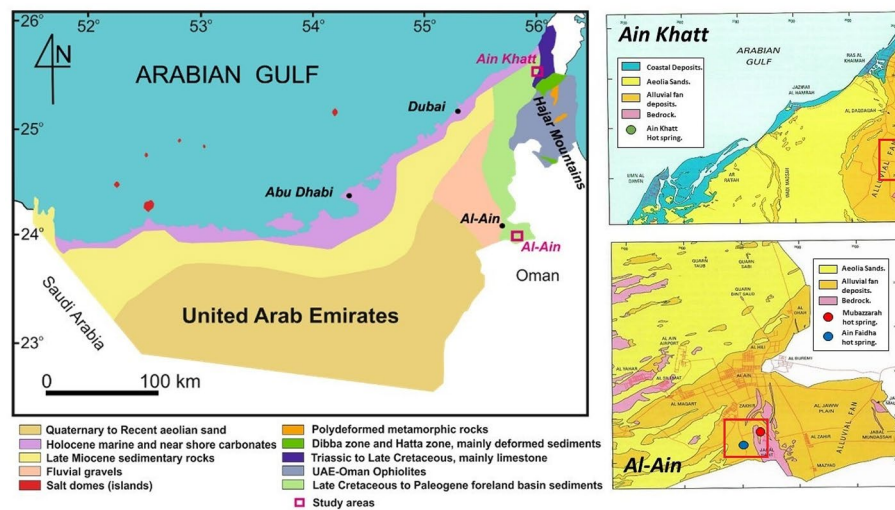


**Fig. 1** Geological map of the UAE showing the locations of the studied geothermal fields, together with the gravity and magnetic survey locations. Green-Mubazzarah–Ain Faidha hot springs are in Al-Ain city and Ain Khatt in Khatt city

## Geological settings

The first study area includes Green Mubazzarah and Ain Faidha, two hot springs located south of Al Ain (Fig. 1), near the northern terminus of the western flank of the Mount Hafit. Mount Hafit is the main geologic feature in this area. It is an anticline that extends for 30 km in a NNW–SSE direction, and is approximately 4.5 km wide. The stratigraphic sequence exposed in Mount Hafit is represented by a thick accumulation of limestones and marl, ranging in age from early Eocene to Miocene. The folding at Hafit dates to the Oligocene (Zagros orogeny) (Stampfli and Borel 2002; Agard et al. 2011; Jolivet and Faccenna 2000). This area is affected by two dominant fracture systems, an E–W system (Sirat et al. 2007; Zaineldeen and Fowler 2014) followed by younger fractures with N–S to NNE–SSW orientations (Zaineldeen and Fowler 2014).

The discharge temperature of hot waters from Green-Mubazzarah–Ain Faidha (GM–AF) springs at the surface ranges from 32 °C to 49 °C. The waters are sodium chloride water type (Saibi et al. 2021a). Saibi et al. (2021a) calculated the temperature of the deep geothermal fluid beneath GM–AF to be around 151 °C.

Ain Khatt (AK), the second study area, is located in the northern part of the UAE, in a mountain village located southeast of Ras Al Khaimah (RAK) city, adjacent to the ophiolitic Hajar Mountains (Fig. 1). The chemistry of the spring waters is Na–Ca–Cl water type (Saibi et al. 2021a). The discharge temperature at these springs is 39 °C. Saibi et al. (2021a) calculated the temperature of the geothermal reservoir beneath AK to be around 112 °C.

Ain Khatt springs are dominated by N–S trending mountain ridges. The Hajar Mountains are the highest parts of the UAE, with peaks reaching above 2000 m ASL. The Hajar Mountains were formed by the same two events responsible for the formation of Mount Hafit (Searle et al. 1983; Searle 1988). As a result of the complex tectonic history, the present Hajar Mountains consist of number of tectono-stratigraphic

units (Breton et al. 2004). There is a Palaeozoic–Mesozoic (pre-Permian to Cretaceous) carbonate shelf sequence, which is overthrust by oceanic sediments (Hawasina Nappes) and oceanic crust (Semail Ophiolite). The Musandam Mountains, which extend northeast of the Hajar Mountains, are mainly composed of the Palaeozoic–Mesozoic carbonates. The Hawasina nappes and the Semail Ophiolite were emplaced during the late Cretaceous (Glennie et al. 1974). The modern topography developed during the later Zagros orogenic event (Breesch et al. 2009).

The UAE–Oman mountain range has influenced the climatic conditions and drainage patterns in the UAE. In the Pleistocene, alluvial sediments accumulated in the wadis at the base of the Musandam Mountains (Al-Farraj and Harvey 2000). Wadis of various sizes dissect the limestone mountain ranges. The study area is dominated by carbonate rocks of Permian to Cretaceous age (Rus El Jibal, Elphinstone, Musandam and Thamama Groups) (Hudson and Chatton 1959; Hudson 1960). Figure 2 shows the lithostratigraphic column of the Northern Emirates in UAE after Abdelghany (2006).

## Methodology and results

### Potential field surveys (Green-Mubazzarah–Ain Faidha, Al-Ain city, Abu Dhabi Emirate)

Magnetic and Gravity surveys were carried out at the Green-Mubazzarah–Ain Faidha geothermal manifestations and in the surrounding areas during 2017 (Fig. 3a).

The gravity surveys were acquired using a Scintrex CG-6 Autograv microgravity meter. The gravity surveys included 273 gravity stations with spacing ranging from 500 m to 4000 m, depending on accessibility. The observed gravity was corrected for tides, tilts, drift, topography, and temperature (Appendix). Figure 4 shows the Bouguer anomaly map for the Al-Ain study area. A residual Bouguer anomaly map was created by using

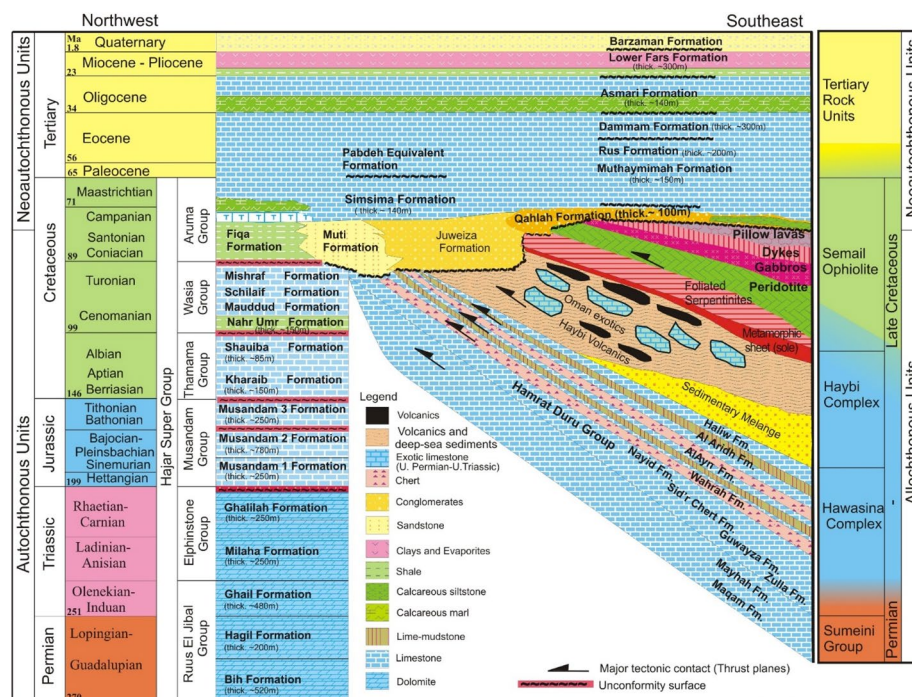


**Fig. 2** Lithostratigraphic chart of the Northern Emirates (Abdelghany 2006)



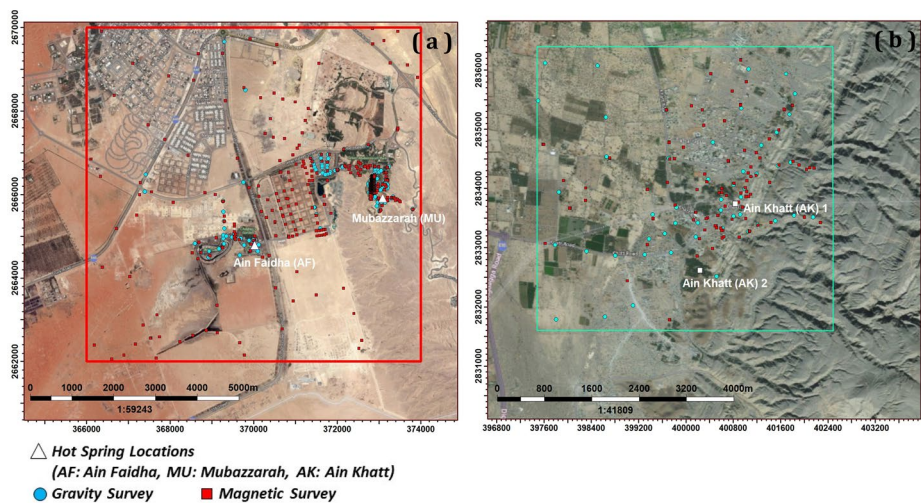


**Fig. 3** a Gravity and magnetic stations at Green Mubazzarah and Ain Faidha and surroundings areas. b Gravity and magnetic stations at Ain Khatt. The coordinates are in UTM (m) for easting (x axis) and northing (y axis)

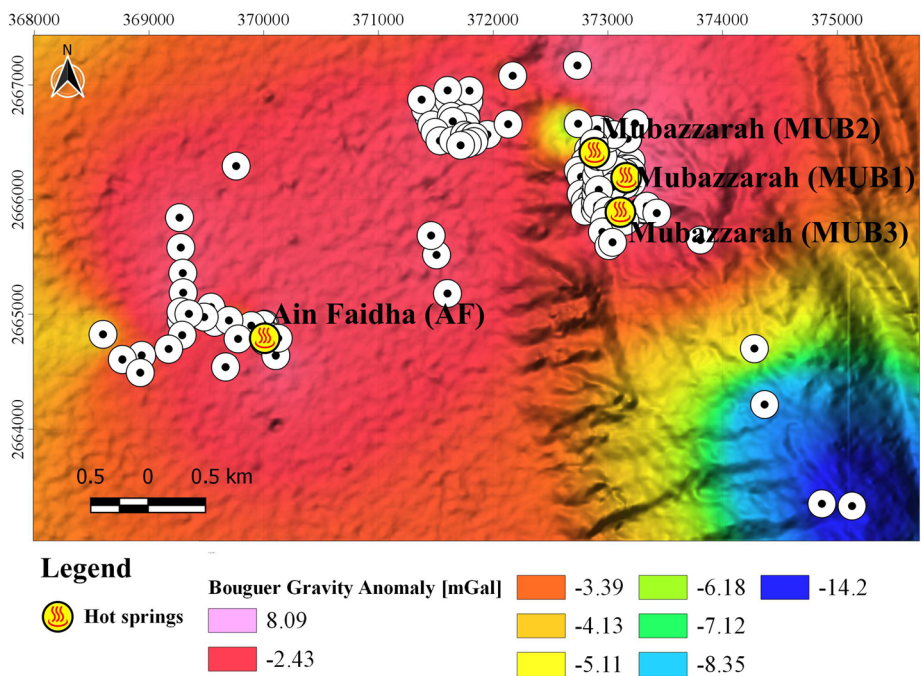


**Fig. 4** Complete Bouguer anomalies (CBA) of GM-AF. The circle symbols show the locations of the gravity data points

the third-order polynomial technique (Fig. 5). The HD and INH techniques were also applied to the Bouguer anomaly data to delineate the subsurface structures (Figs. 6 and 7, respectively).

The magnetic data were acquired using a Geometrics G-856 AX Proton magnetometer. The total number of magnetic stations is 603 stations with a spacing interval ranging from 10 to 1500 m, depending on accessibility, which was sometimes limited due

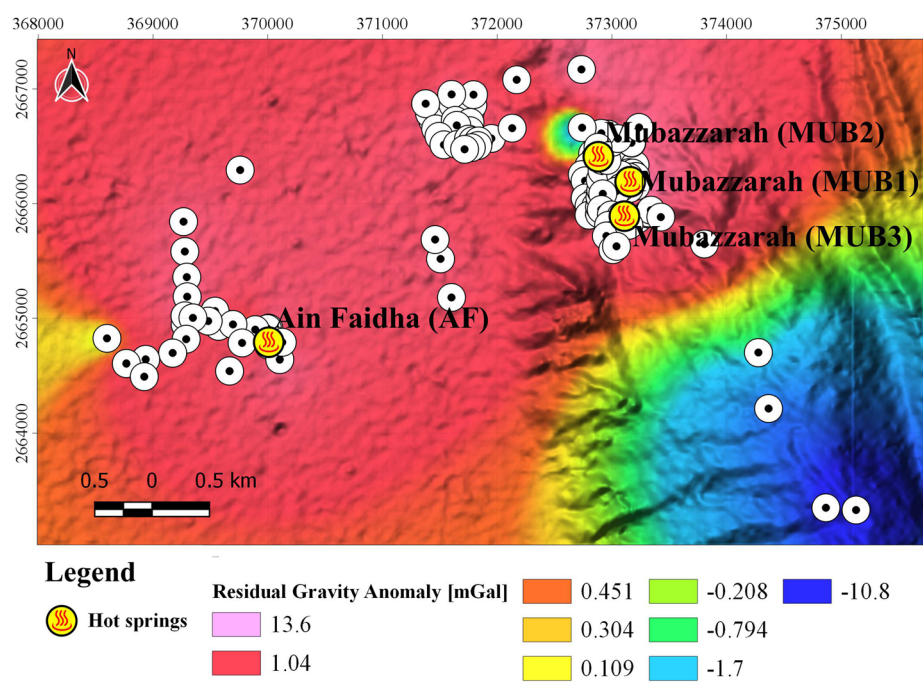


**Fig. 5** Residual Bouguer anomaly map of GM–AF calculated from the CBA using bilinear interpolation

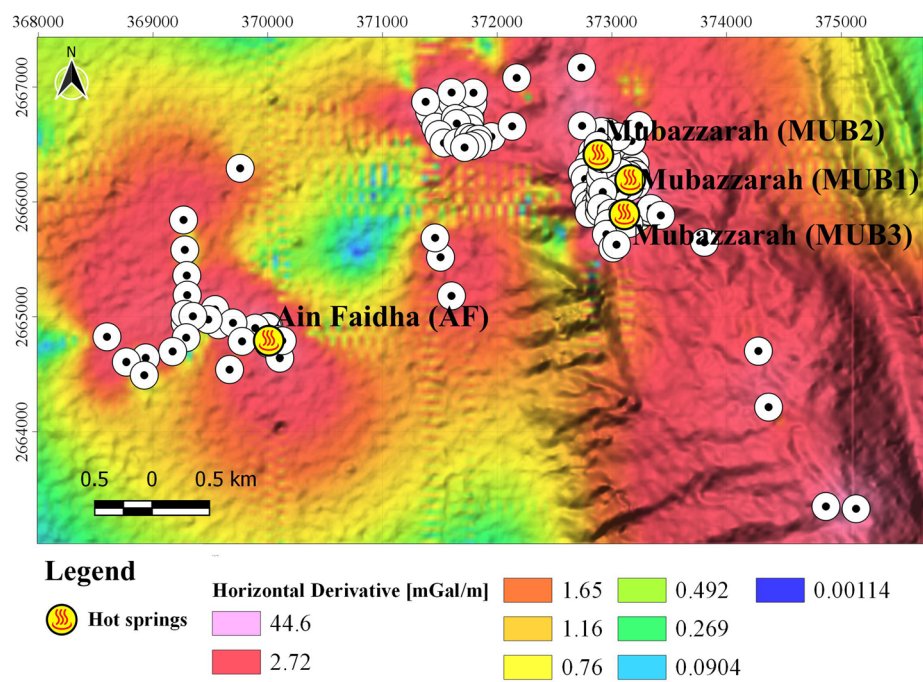


**Fig. 6** HD values of the Bouguer anomaly of GM–AF. The maxima of HD values show the locations of contacts/faults



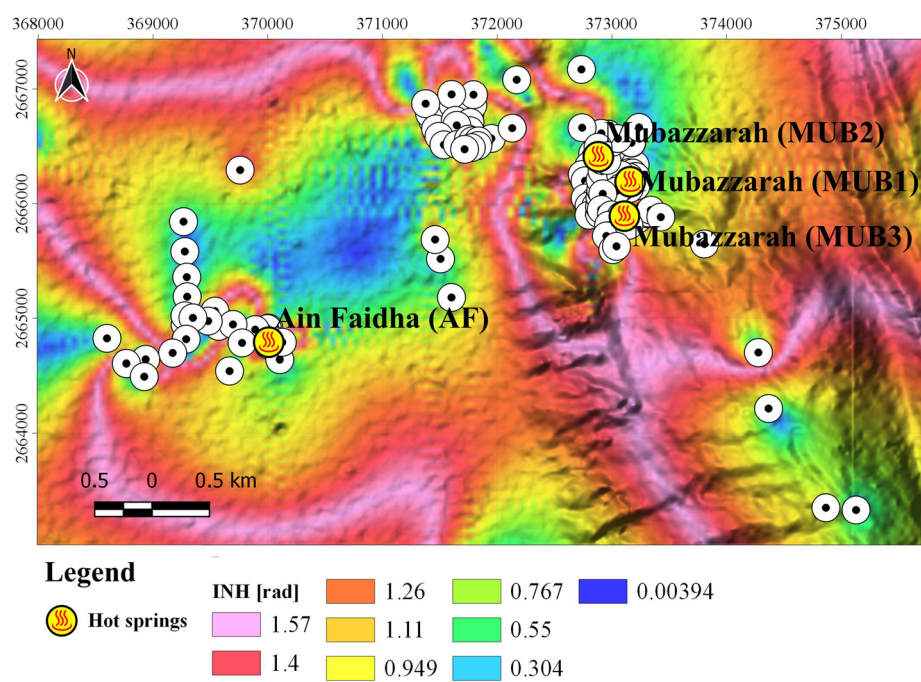


**Fig. 7** INH map of the Bouguer anomaly of GM–AF. The maxima of the INH values represent the locations of contacts/faults

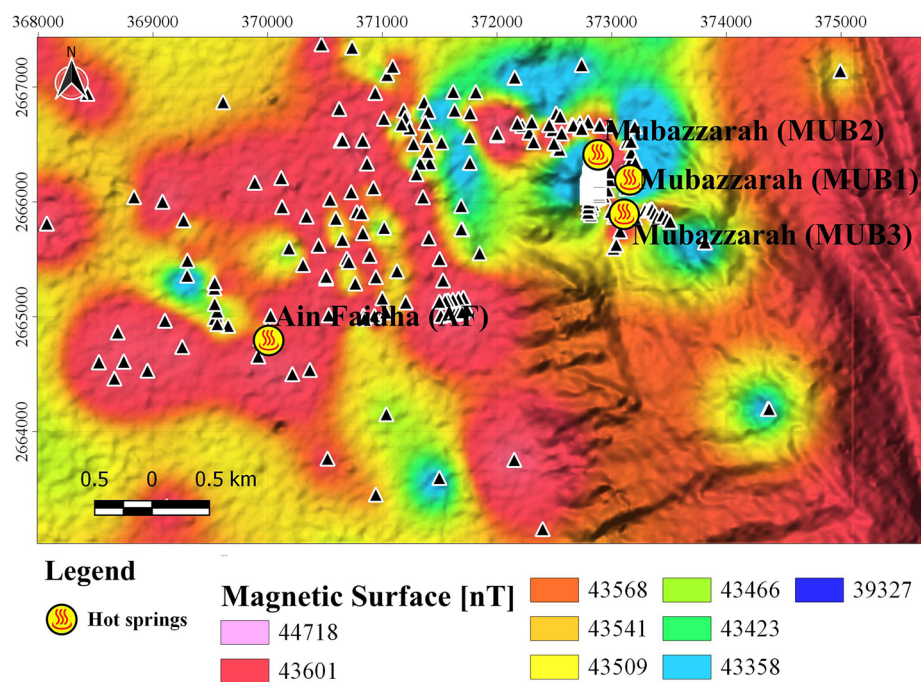


**Fig. 8** Magnetic map of GM–AF. The triangle symbols show the locations of the magnetic data points

to the presence of sand dunes or zone restrictions (private and military). The observed magnetic data have been corrected for the temporal variations of the magnetic field. In the processing, we calculated the base drift and diurnal change rate then subtracted the diurnal correction from the observed magnetic reading. The result is the study region total magnetic intensity (TMI) map (Fig. 8).

The residual magnetic field map is calculated by subtraction of the regional component (i.e., IGRF) from the RTP magnetic anomaly data (Fig. 9). The HD and INH techniques are applied to the magnetic data to delineate the subsurface structures (Figs. 10 and 11), respectively.

All applied corrections and methods are presented in the [Appendix](#).

#### Potential field data (Ain Khatt, Khatt city, RAK Emirate)

The gravity survey was acquired during 2017 using the Scintrex CG-6 Autograv microgravity meter (see Fig. 3b). The gravity survey included 65 gravity stations that concentrated on the area of interest. The observed gravity data were corrected following the same procedure as described for Al-Ain geothermal system. Figure 12 shows the Bouguer anomaly map for the Ain Khatt area. A residual Bouguer anomaly map was created using the third-order polynomial technique (Fig. 13). The HD and INH techniques were also applied to the Bouguer anomaly data to delineate the subsurface structures (Figs. 14 and 15, respectively).

The magnetic survey was acquired during the same period and the total number of magnetic stations is 109 with a spacing interval ranging from 0.5 km to 1.5 km, taken in accessible locations (see Fig. 3b). The magnetic data were corrected following the

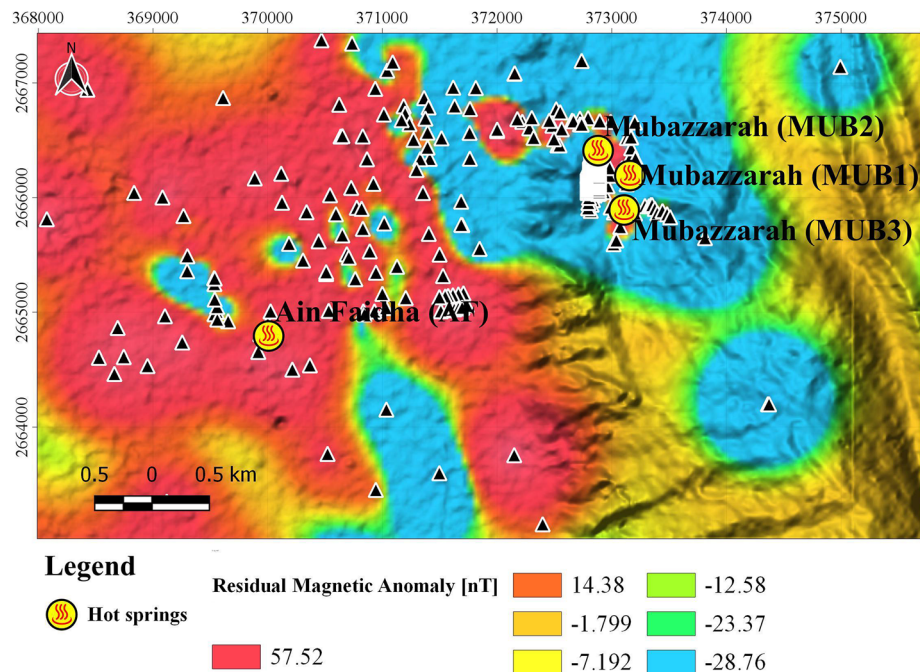


**Fig. 9** Residual magnetic map of GM-AF. The triangle symbols show the locations of the magnetic data points



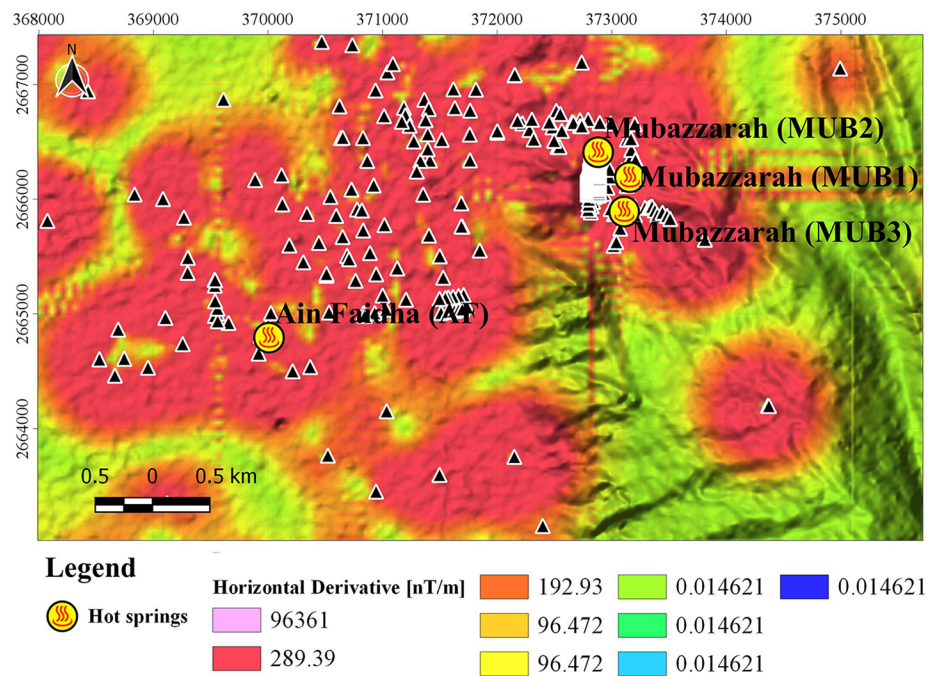


**Fig. 10** HD values of the magnetic map of GM–AF. The maxima of HD values show the locations of contacts/faults

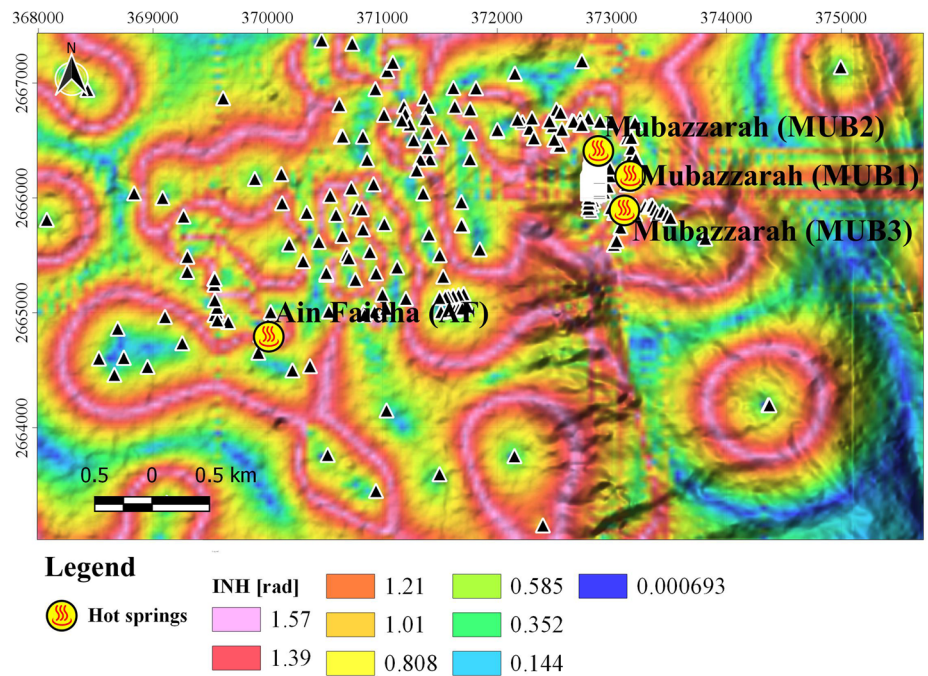


**Fig. 11** INH map of the magnetic map of GM–AF. The maxima of the INH values represent the locations of contacts/faults

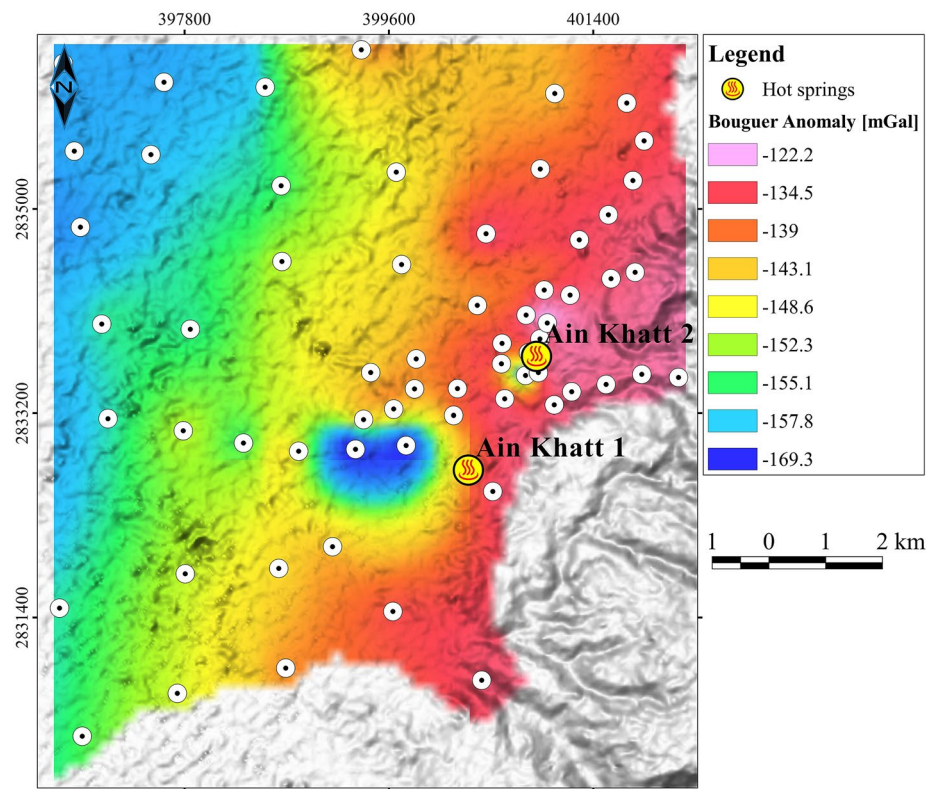


**Fig. 12** Complete Bouguer anomalies (CBA) of AK. The circle symbols show the locations of the gravity data points

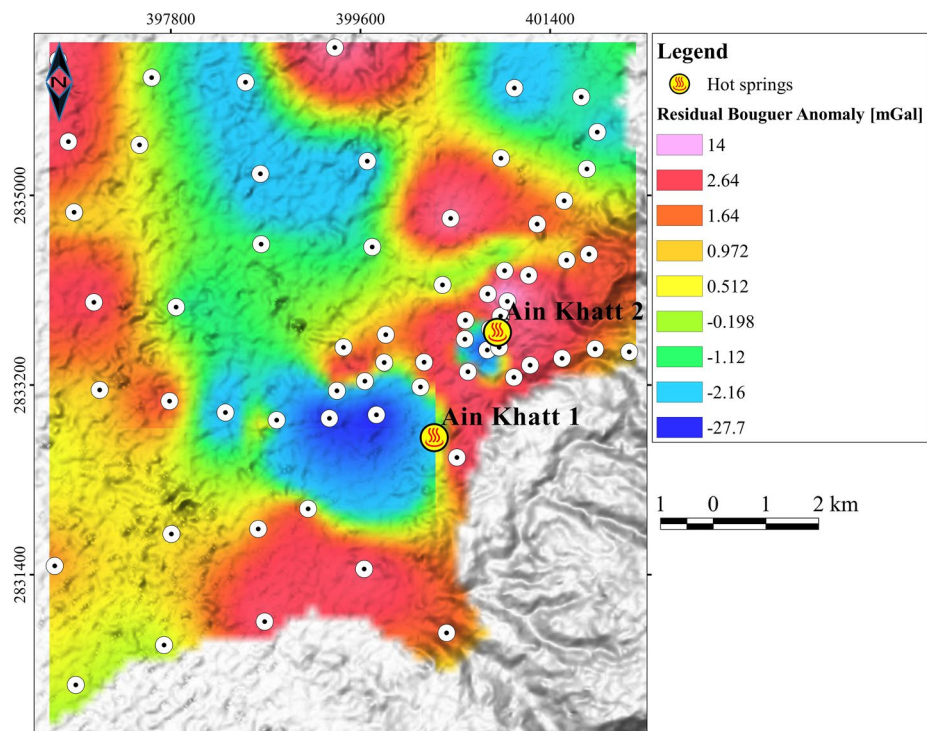


**Fig. 13** Residual Bouguer anomaly map of AK calculated from the CBA using bilinear interpolation



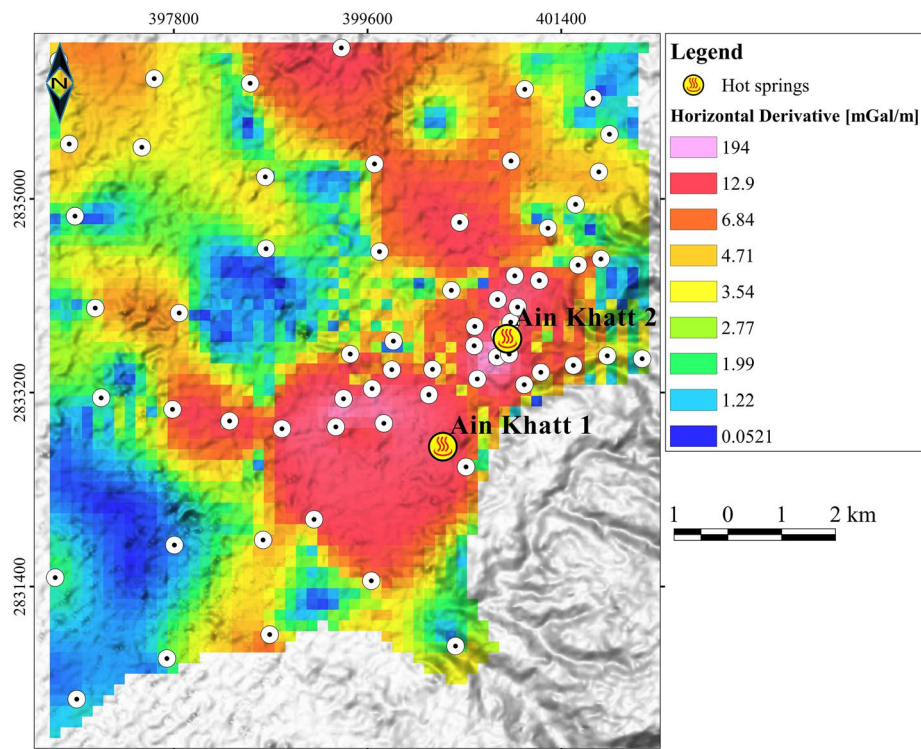


**Fig. 14** HD values of the Bouguer anomaly of AK. The maxima of HD values show the locations of contacts/faults

same procedure as described for Al-Ain geothermal system. The TMI map is shown in Fig. 16. The residual magnetic map is presented in Fig. 17. The HD and INH techniques again were applied to the magnetic data to delineate the subsurface structures (Figs. 18 and 19, respectively).

### Three-dimensional gravity and magnetic inversion and Neural Network modeling

For a better understanding of the subsurface structure of the geothermal fields at Al-Ain and Ain-Khatt, we assessed the 3D subsurface structure using inversion for both gravity and magnetic data. Inversion is calculated using the gravity and magnetic inversion toolkit of the Petrel software (Petrel 2022). Gravity inversion estimates the three-dimensional density contrast distribution of the subsurface, allowing the delineation of the subsurface structural features, while the magnetic data inversion underlines the magnetic susceptibility of the hydrothermal activity. Interpretation of these two physical parameters helps to draft an initial 3D structural subsurface model of the geothermal fields.

The inversion technique, applied to develop the 3D models of magnetic susceptibility and density contrast, was published by Priezzhev (2005, 2010), Kobrunov and Varfolomeev (1981), and Kobrunov (2007). The inversion method begins with the creation of a 2D grid model (surface) of the potential field data. The model is the basis of the 3D spatial distribution of the magnetic susceptibility and density characteristics in the

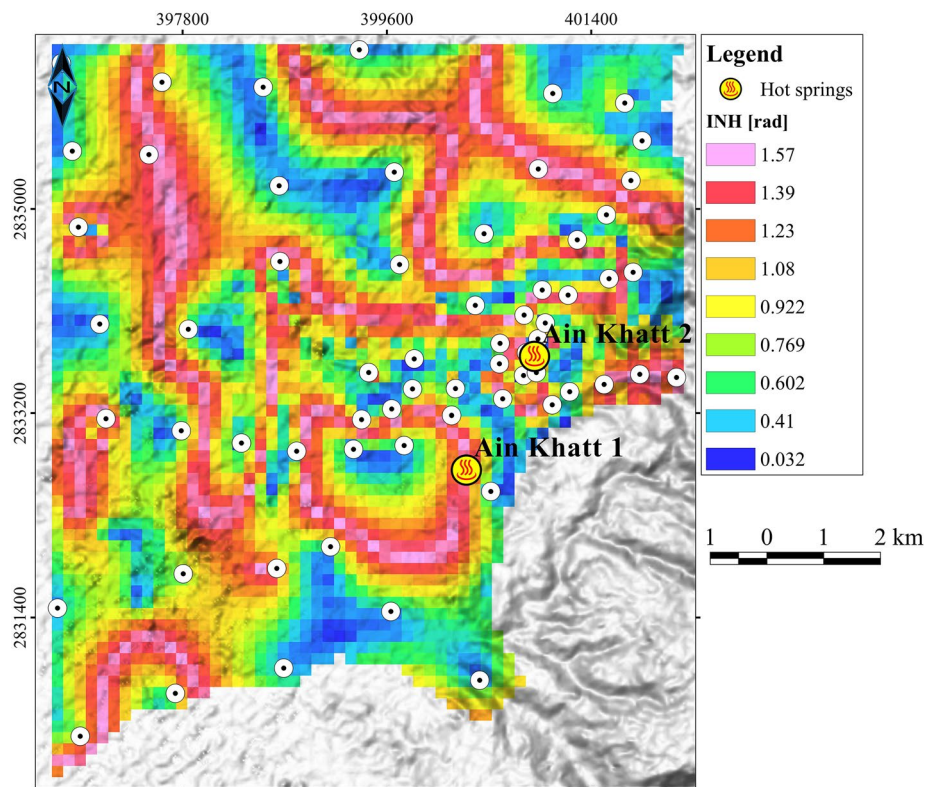


**Fig. 15** INH map of the Bouguer anomaly of AK. The maxima of the INH values represent the locations of contacts/faults

wavenumber domain. 3D wavenumber domain inversion is much like 3D convolution in having a single unique solution. For details about the mathematics of the method, see Priezzhev and Pfitzner (2011). Measured gravity and magnetic data are interpolated into surfaces and used separately for 3D inversion down to 2000 m depth for Green-Mubazzarah–Ain Faidha, and 1200 m depth for Ain Khatt with a vertical sampling interval of 5 m. Inversion results of both gravity and magnetic data are illustrated as transverse sections crossing the main hot springs areas at both Al-Ain and Ain Khatt (Fig. 20) (Additional file 1).

In Al-Ain city, a transverse vertical section crossing both Ain Faidha and Green-Mubazzarah hot springs shows the geological substructure beneath the geothermal fields. The density distribution (Fig. 20a) shows a remarkable low-density contrast (blue color) occurring as an undulating structure down to 750 m, apparently connecting Ain Faidha to Green-Mubazzarah. This low-density anomaly is interpreted as a local high fracture density zone shaped by brittle structures visible at the surface. Similarly, the magnetic susceptibility inversion along the same section (Fig. 20b) shows a high susceptibility zone (green color) coinciding with the main zone of oscillating of the water table, and in this zone, permeability controlled iron hydroxide alterations can produce similar undulating high and low magnetic susceptibility patterns. These inversion results suggest that the hot springs at Ain Faidha are fed by the same thermal water conduits that like closer to Mount Hafit. The Ain Khatt hot spring density distribution beneath AK1



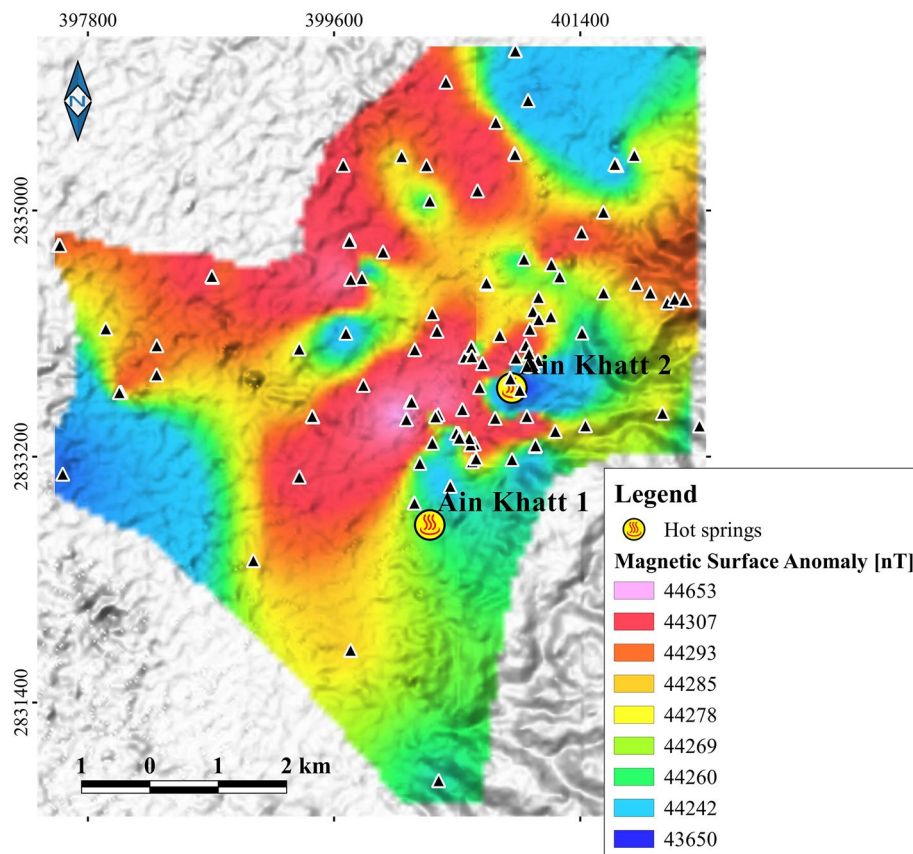


**Fig. 16** Magnetic map of AK. The triangle symbols show the locations of the magnetic data points

and AK2 (Fig. 20c) shows extensive density contrasts near the surface, shaping a structure similar to the one observed in Al-Ain city hot-springs, while the magnetic intensity inversion (Fig. 20d) highlights a less prominent water upflow zone from depth.

It is possible to retrieve the subsurface structural model from both gravity and magnetic inversion results simultaneously. For this purpose, we used a trained estimation neural network-based model that extracts the common geometrical features from both gravity and magnetic results. Artificial Neural Networks (ANN) are powerful interpretation tools for data classification and clustering that can be applied for a variety of geological interpretations. Classification guides the computation of discrete data, and both supervised and unsupervised training data can be applied. It will estimate the probability of the input instead of estimating the class that each point is assigned to. The highest probability class is assigned to that point. Regularities and trends are identified by the classification method using input data. The method makes modifications based on neural network function. The method optimizes and organizes the output, and the self-organizing process determines the parameters. A characteristic feature of a neural network is that it learns by example. Therefore, we must provide the network with a training set of both gravity and magnetic data. We trained an unsupervised ANN classification to subdivide the common structural geological features from the magnetic susceptibility and density

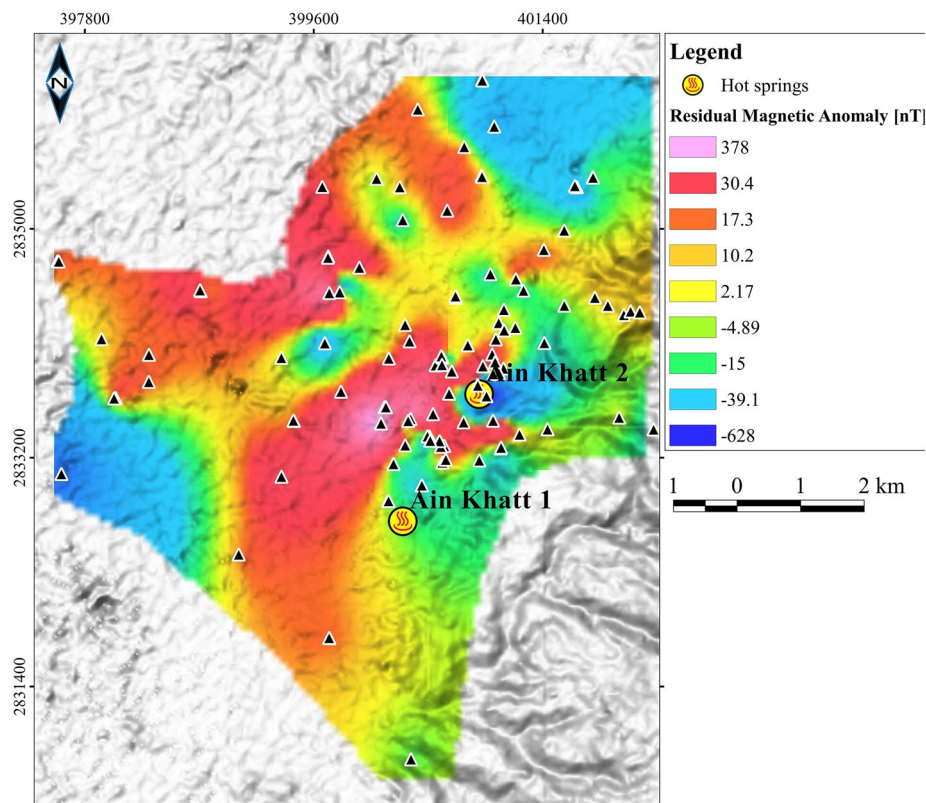


**Fig. 17** Residual magnetic map of AK. The triangle symbols show the locations of the magnetic data points

distribution from 300 iterations. Three independent trainings and classifications were performed, from which we estimated the average structural mean in order to avoid any deficiency of the physical interpretation. The averaged structural model estimations for both Green-Mubazzarah and Ain Khatt are summarized in Fig. 21. Plotting of the error function against iterations (Fig. 21a and c) shows that the algorithm reaches its best misfit at around the 280th epoch, where it stabilizes at its best value. Average models from 3 classifications, and a cross-section are illustrated for Green-Mubazzarah–Ain Faidha geothermal field (Fig. 21b) and Ain Khatt (Fig. 21d).

## Discussion

The Bouguer gravity values in GMAF and AK show ranges from  $-14.2$  to  $8.09$  mGal and  $-169.3$  to  $-122.2$  mGal, respectively (Figs. 4 and 12). The TMI values for the geothermal fields GMAF and AK vary from  $39,327$  to  $44,718$  nT and  $43,650$  to  $44,653$  nT, respectively (Figs. 8 and 16). The GMAF hot springs (MUB1, MUB2, MUB3 in Fig. 8) are located at boundaries between high and low magnetic domains, except for the Ain Faidha hot spring, which is located in a high magnetic region (AF in Fig. 8). Ain Khatt hot springs (Ain Khatt 1 and Ain Khatt 2) are located in intermediate and low magnetic regions (Fig. 16). In the HD maps from Bouguer and TMI data in GMAF, the hot springs (AF, MUB1, MUB2, MUB3) are located in high HD value regions (Figs. 6 and 10). On the other hand, the INH maps calculated from gravity

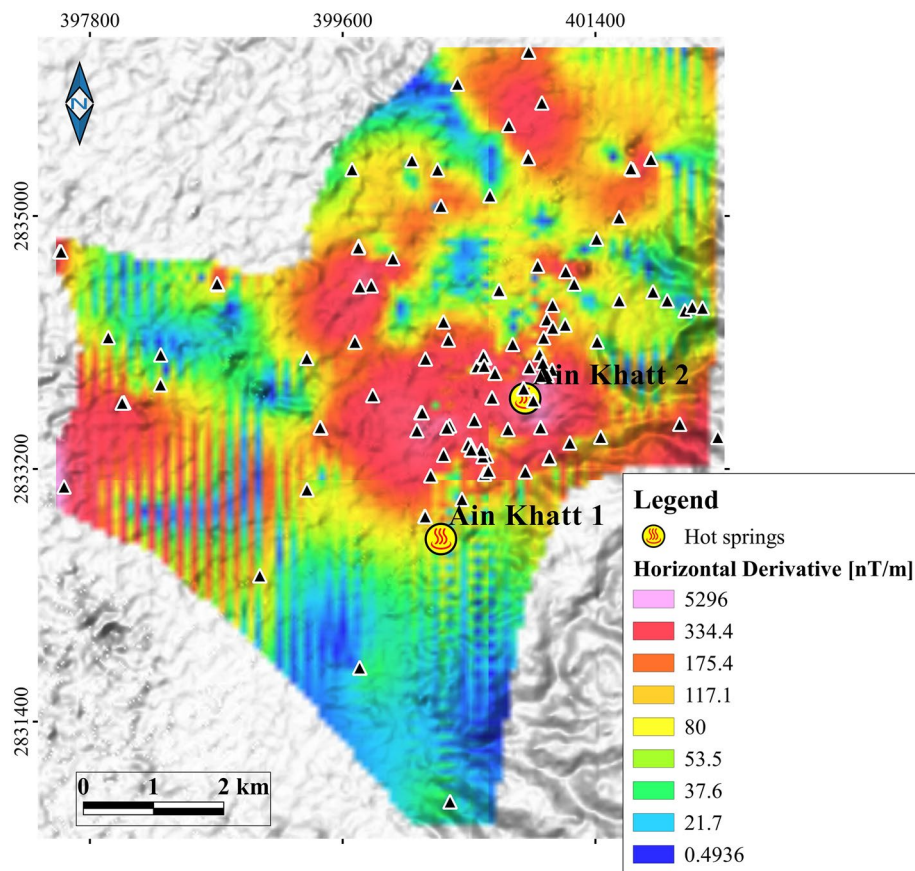


**Fig. 18** HD values of the magnetic map of AK. The maxima of HD values show the locations of contacts/faults

and magnetic data from GMAF show that Al-Ain hot springs are located at high INH values (Figs. 7 and 11).

In the HD maps from Bouguer and TMI data from Ain Khatt, the hot springs (Ain Khatt 1 and Ain Khatt 2) are located in high HD value regions (Figs. 14 and 18) except Ain Khatt 1 in HD calculated from magnetic data, is located at low HD region (Fig. 18). For the INH maps calculated from gravity and magnetic data from Ain Khatt geothermal field, the Ain Khatt hot springs are located at high INH values or near high INH values (Figs. 15 and 19). In general, the UAE hot springs emerge at points along or near geological contacts.

The inversion results, prepared from potential field data, showed that the hot springs emerging at GMAF and AK are structurally controlled by vertical contacts/faults with depths ranging from 200 m below sea level (BSL) at AK to 2000 m BSL at GMAF.

The low-enthalpy geothermal systems hosting the Al-Ain and RAK hot springs are themselves enclosed in areas bordering large tectonic structures. The Al-Ain geothermal area lies at the edge of the Mount Hafit anticline, while the RAK geothermal area near Khatt City, RAK, lies near the Semail Thrust at the foothills of the Hajar Mountains.



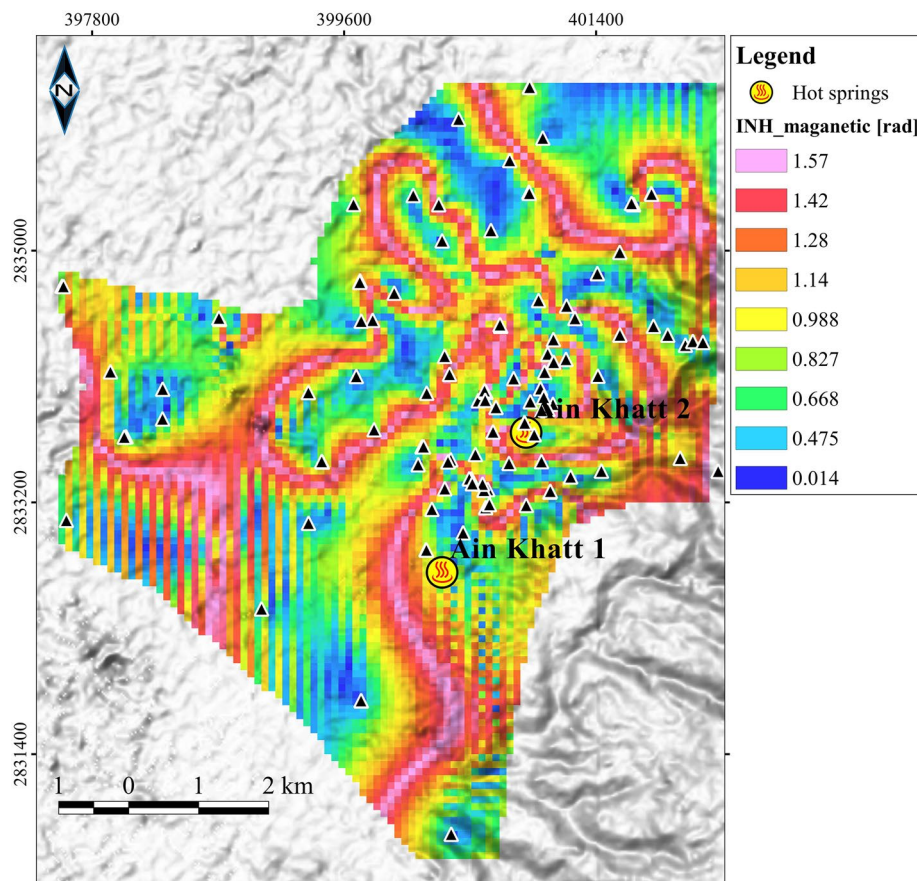


**Fig. 19** INH map of the magnetic map of AK. The maxima of the INH values represent the locations of contacts/faults

Within these respective geothermal areas, the locations of hot springs emanations appears to be controlled by fracture systems (primary, e.g., lithological contacts, and secondary, e.g., faults). The anomalous geothermal aspects of the studied areas are probably a result of advection of hot groundwater within zones of higher than normal fracture intensity, and with deep fracture penetration. The high fracture density in the core of the Mount Hafit anticline has been reported by Zaineldeen and Fowler (2014). In the core of the mountain, fossil groundwater circulation systems are represented by calcite veins linked to karstic dissolution features. It is likely that the focus of hot springs activities has migrated with time along a major E–W fracture dissecting the anticline, so that now the springs emerge on the western limb of the anticline.

Precise control of the location of the springs at the surface is difficult to determine. However, the U-shaped magnetic anomaly may reflect intersecting zones of limonitized fault marginal zones controlled by subtle permeability variations along E–W fault planes which dip to the north or south steeply. Progressive water table seasonal and secular variations of the walls of the conduits for the hot springs would produce a complex pattern of limonite alteration of fault margins.

AK geothermal area lies west of the Musandam Mountains, locally consisting of steeply dipping Thammama and Musandam Group limestones. These are overlain by



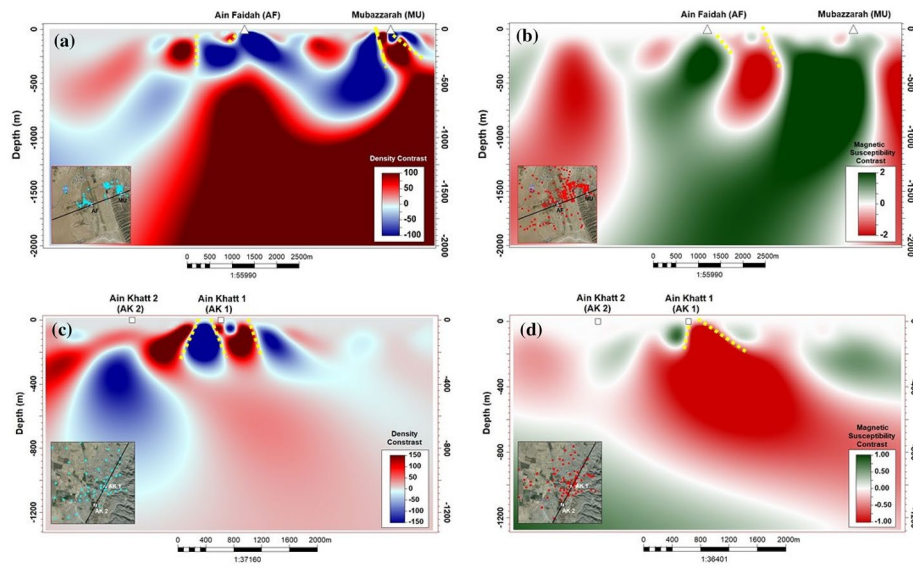


**Fig. 20** Potential field inversion results at Al-Ain and Ain Khatt hydrothermal locations. Dashed yellow lines are interpreted faults. **a** Density contrast section of Green-Mubazzarah-Ain Faidha hot springs in Al-Ain city. **b** Magnetic susceptibility section of Green-Mubazzarah-Ain Faidha hot springs in Al-Ain city. **c** Density contrast section of Ain Khatt hot spring in RAK. **d** Magnetic susceptibility section of Ain Khatt hot spring in RAK

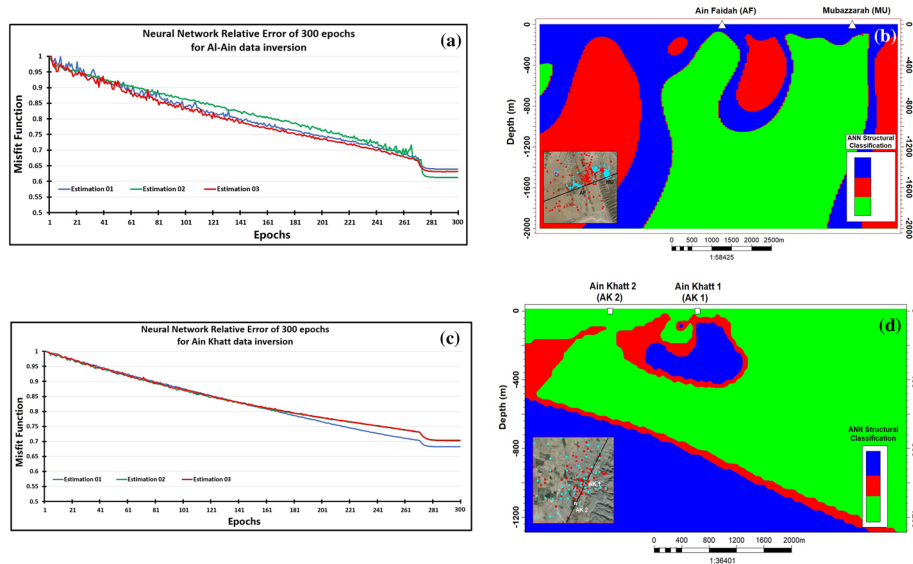


**Fig. 21** Neural Network classification results. **a** ANN relative error function from 3 estimations at Green-Mubazzarah-Ain Faidha hot spring in Al-Ain city. **b** ANN structural modeling of Green-Mubazzarah-Ain Faidha hot spring in Al-Ain city. **c** ANN relative error function from 3 estimations of Ain Khatt hot spring in RAK. **d** ANN structural modeling of Ain Khatt hot spring in RAK

Miocene alluvial fan conglomerates that are known to be important aquifers. The AK1 and AK2 springs lie along a NNE-trending line that parallels deep strike-slip faults in the mountains to the east. The probability is that the springs are controlled by these

NE-trending faults. The area is presently covered by thick Holocene alluvium obscuring bedrock structures.

## Conclusion

Dense gravity and magnetic observations were carried out at and around the main geothermal fields in UAE, Green-Mubazzarah–Ain Faidha in Al-Ain city and Ain Khatt in Khatt city to highlight the 2D and 3D subsurface structure, using HD, INH and 3D inversion techniques. The 2D analysis (HD and INH) of gravity and magnetic data showed that the hot springs lie close to geophysically interpreted faults. This can explain the reason of geothermal discharge being located in these areas. The 3D joint gravity and magnetic inversion results showed that the depth extension of such interpreted faults reaches around 2 km or greater. The 3D gravity–magnetic ANN joint inversion assisted in imaging the 3D shape bodies of high density and high magnetic susceptibility beneath the Green-Mubazzarah–Ain Faidha hot springs, which resemble elongated lobes developed along fault planes and at fault intersections. Previous geological studies demonstrated the existence of E–W and NNW–SSE faults and highly fractured zones in this area that can act as conduits for hot waters.

## Appendix

### Magnetic method

The geomagnetic field of the Earth is complex with changes in time, space, direction, and intensity. The geomagnetic field at the surface of the Earth is considered to result from two processes. The first is from the Earth's interior (internal magnetic field), and the second from beyond the Earth (external magnetic field) (Le Mouél 1969).

The main or dipole field (which constitutes 99% of the measured field at the surface represents the internal field. Its origin is due to complex deep-seated magneto-fluid dynamic processes and the crustal field generated by magnetized rocks. The external field is generated by electric currents in the ionosphere and in the magnetosphere.

The magnetic field measured at the surface ( $T_{obs}$ ) is the sum of three components:

$B_n$ : The main or regular magnetic field, which corresponds to large wavelength anomalies (over thousands of kilometers) with intensity of several thousand nT.

$B_a$ : A magnetic anomaly field that corresponds to short wavelength magnetic anomalies (over a few thousands of meters) and generally with maximum amplitude of the order of hundreds nT.

$B_t$ : Transient or temporary field, with much lower and variable intensity with the time. It originates mainly from external sources.

In a surface magnetic survey, only the magnetic anomaly field is of practical interest, and can be obtained according to the following equation:

$$|B_a| = |T_{obs}| - |B_n| + |DB_t|.$$

### Elements of the geomagnetic field

The Earth's magnetic field is a vector quantity,  $\vec{B}$  with properties of direction and intensity. In the spherical coordinate system, the components of the field ( $B_r$ ,  $B_\theta$ , and  $B_\phi$ ) are given by complex relationships.

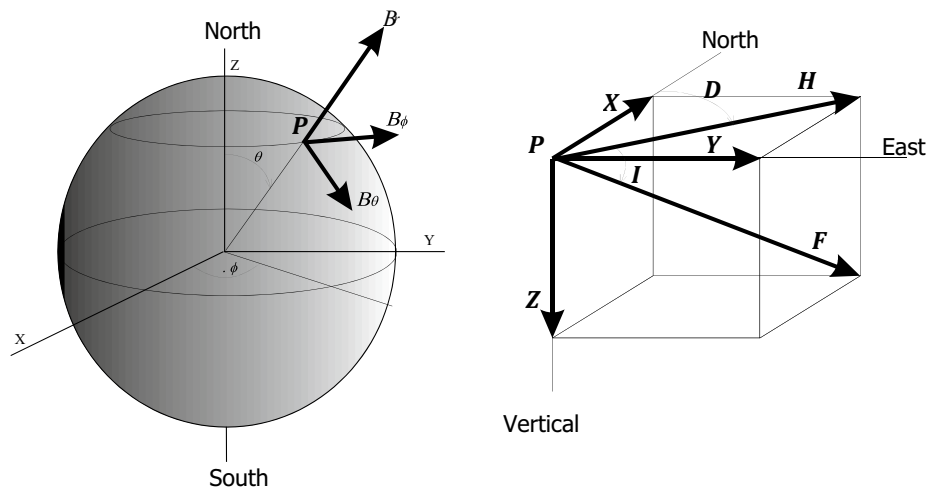


**Fig. 22** Elements of the geomagnetic field at a point P in **a** the spherical coordinate system and **b** Cartesian coordinate system

The full determination of the magnetic field at a point in space necessitates measurement of three independent elements that can be chosen from among the seven following (Fig. 22):

1. The North component  $X = -B_\theta$ .
2. The East component  $Y = B_\phi$ .
3. The vertical component  $Z = -B_r$ .
4. The declination  $D$ : angle between the Magnetic Meridian and the Geographic Meridian, is positive or "East" when the magnetic meridian is to the East of the Geographic Meridian, and is given by one of the following formulae:

$$D = \arctan(Y/X) \text{ or } D = \arcsin(Y/H).$$

5. The inclination  $I$ , angle between the field vector and the horizontal plane, is positive when the field vector points towards the center of the earth (Northern Hemisphere). It is expressed by:

$$I = \arctan(Z/H).$$

6. The total  $F$  (or sometimes  $T$ ) is the intensity of the magnetic field. It is given by the following formula:

$$F = \sqrt{X^2 + Y^2 + Z^2}.$$

The intensity of the horizontal component  $H$  is expressed by the Cartesian components  $X$  and  $Y$  (North and East, respectively) and is given by the following formula:

$$H = \sqrt{X^2 + Y^2}.$$

### International magnetic reference field formula (IGRF)

The mathematical representation models of the geomagnetic field was adopted according to an internationally agreed protocol under the auspices of the International Association of Geomagnetism and Astronomy (IAGA), which is a branch of the International Union of Geodesy and Geophysics (IUGG). These models known as the IGRF (International Geomagnetic Reference Field) are models of global reference, calculated every 5 years. The models are rounded off to the tenth of a degree for the geomagnetic field and to the eighth of a degree for the temporal variations, which correspond to a certain time.

These IGRFs, based on different models, are constructed from data available at a given time then extended by a model of secular variation at the time of the reference model. Due to the fact that it is impossible to predict exactly the variations in the time of the magnetic field, certain discrepancies are noted between the true geomagnetic field and the IGRF model. In the long term, it is possible to correct and improve the former IGRF with the input of data, including satellite collected data.

### Variations of the magnetic field ( $B_t$ )

When field measurements are being taken at a fixed location, it will be noticed that these measurements vary on the time scale of milliseconds to millions of years. Changes in short periods are essentially caused by electric currents in the ionosphere. These temporal variations are known as the diurnal variations. The variations in the long periods have their origin in the Earth's nucleus and are called secular variations. These are often represented on maps indicating the rate of change in nT/year for the intensity of the magnetic field, and in degree/year for the inclination or the magnetic declination.

### Magnetic field of the crust ( $T_{nor}$ )

The spectral analysis of the energy allows the separation of the main field (which is a complex magnetic fluid dynamic phenomena associated with the liquid outer core) from the crustal field, which is associated with the magnet rocks of the Earth's crust.

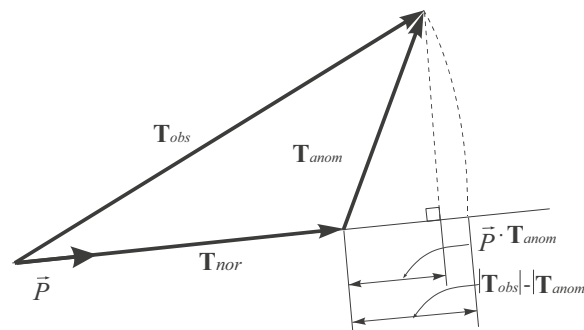


**Fig. 23** Vector representation of the magnetic anomaly field. The  $T_{obs}$  is the vector sum of the  $T_{nor}$  (regional field) and the anomalous field ( $T_{anom}$ ).  $\vec{P}$  is the unit vector of the regional field vector



### Total magnetic field anomalies ( $T_{\text{anom}}$ )

The modern precession magnetometer (proton magnetometer) is used to measure the total magnetic field strength. Total field magnetic anomalies are obtained by subtraction of a regional component (for example the IGRF) from the measured field.

Referring to the anomalous field (magnetic anomalies) due to a certain source, as  $T_{\text{anom}}$ , this quantity can be represented by the following relationship (Fig. 23):

$$T_{\text{anom}} = T_{\text{obs}} - T_{\text{nor}}.$$

The intensity of the magnetic anomaly field is very small compared to that of the normal field ( $|T_{\text{nor}}| \gg |T_{\text{anom}}|$ ). This condition is usually true for crustal anomalies.

The magnetic survey of the study area was acquired using a Geometrics G-856 AX Proton magnetometer. The total number of magnetic stations is 603 with a spacing interval ranging from 10 to 1500 m depending on the accessibility, which was sometimes limited due to the presence of sand dunes or zone restrictions (private and military).

### Reduction to magnetic pole technique

Reduction to the pole (RTP) is a correction that must be applied to the magnetic data before interpretation. If a body is located at the Earth's magnetic poles, it would be geophysically characterized by a magnetic high situated directly above the body. If the body lies anywhere else, the Earth's field produces a magnetic high to the South of a magnetic body in the northern hemisphere, and to the north of a body located in the southern hemisphere. This technique was first developed by Baranov (1957), to correct the position of the magnetic anomalies. The requisite mathematical equations, together with the coefficient of RTP in space domain, have been provided by Baranov and Naudy (1964) and Baranov (1975). The calculations for the RTP are carried out on the total field intensity magnetic data in the space domain by convolving the gridded data with a set of coefficients, the space domain operator has magnetic inclination of  $37.90^\circ$  (the inclination of the study area), and  $1.79^\circ$  declination angle. Equation for the reduction process (Sudhir 1988) is:

$$g' = -\mu T(O) - \frac{1}{2\pi} \iint T(\rho, \omega) \Omega_3(\omega) \frac{d\rho}{\rho} d\omega,$$

where following Baranov's notation:

$$\Omega_3(\omega) = 2 \sum_{\lambda=1}^{\infty} (-\eta)^\lambda k(k + \mu) \cos k\omega,$$

$g'$  = total magnetic field at point  $o$ , reduced to the pole;  $\mu = \sin I$ ,  $I$  being the inclination of the observed magnetic field;  $T(\rho, \omega)$  = total field at the magnetic observation point  $(\rho, \omega)$  (polar coordinates) with reference to the calculation point at the origin where the observed field is  $T(O)$ , and

$$\eta = (I - \sin(I)) / \cos(I).$$

### Residual magnetic anomaly (least square polynomial technique)

The RTP magnetic map includes both regional and residual components. The regional anomalies mask some of the residual anomalies. Therefore, it is necessary to treat each anomaly in a separate map. The magnetic anomalies are separated into regional and residual components, using different techniques. The least square polynomial technique: Nettleton 1976; discussed in this method, consists of subtracting a polynomial surface that approximates the regional component. Agocs (1951) represented the regional field by a uniform plane surface, whereas Fajkiewicz (1959) approximated the regional field by a second order polynomial and concluded that using higher order polynomials might result in the inclusion of part of the residual field in the regional picture. The regional component can be represented by each of the following polynomial surfaces (orders 1 to 3):

$$Z_1(x, y) = \sum_{n=0}^1 \sum_{s=0}^n a_{n-s,s} x^{n-s} y^s \quad \text{plane surface,}$$

$$Z_2(x, y) = \sum_{n=0}^2 \sum_{s=0}^n a_{n-s,s} x^{n-s} y^s \quad \text{second-order surface,}$$

$$Z_3(x, y) = \sum_{n=0}^3 \sum_{s=0}^n a_{n-s,s} x^{n-s} y^s \quad \text{third-order surface,}$$

where  $Z$  is the regional component,  $a_{n-s,s}$  are  $\frac{1}{2}(P+1)(P+2)$  coefficients;  $P=1, 2$  or  $3$  is the order of the two-dimensional polynomials,  $x$  and  $y$  are the coordinates.

Also, the residual component can be separated by subtracting the previously obtained IGRF from the RTP map.

### The improved normalized horizontal tilt angle (INH)

The improved normalized horizontal tilt angle (INH) method helps in locating geological boundaries and magnetic/gravity source edges. The equation is given Li et al. (2014):

$$\text{INH} = \tan^{-1} \left\{ \sqrt{\left(\frac{\partial P}{\partial x}\right)^2 + \left(\frac{\partial P}{\partial y}\right)^2} / a + \left| \frac{\partial P}{\partial z} \right| \right\},$$

where  $P$  is the potential field (gravity field and magnetic field) and  $a$  is a positive constant value and is decided by the interpreter.

### Horizontal derivative (HD)

The HD was developed by Cordell and Grauch (1985), where:

$$\text{HD} = \sqrt{\left(\frac{\partial P}{\partial x}\right)^2 + \left(\frac{\partial P}{\partial y}\right)^2}, \text{ and } P \text{ is the potential field (gravity field and magnetic field).}$$

### Gravity corrections and Bouguer anomaly

Bouguer anomaly at each station is given by:

$$g = G_{abs} - \gamma + F - 2\pi G\rho H + T_c\rho = G_{abs} - \gamma + (\beta - 2\pi G\rho)H + T_c\rho.$$

$g$  is Bouguer anomaly,  $G_{abs}$  is absolute gravity at the station,  $\gamma$  is normal gravity,  $F = \beta H$  is free-air correction,  $2\pi G\rho H$  is Bouguer correction,  $T_c\rho$  is terrain correction.

### Gravity terrain correction

Terrain correction considers topography up to 60 km from each station. The effect of terrain is greater at closer area. Therefore, we use more precise terrain model at closer area. For terrain correction up to 20 m from the station, the correction is calculated assuming that terrain around the gravity station is two dimensional. For terrain correction from 20 m to 60 km from the station, the correction is calculated based on Hammer method using DEM (SRTM). We have used a computer code developed by Komazawa (1988) for gravity terrain corrections. More details about gravity corrections can be found at Saibi et al. (2019a, b).

### Supplementary Information

The online version contains supplementary material available at <https://doi.org/10.1186/s40517-022-00240-4>.

**Additional file 1.** 3D inversion of gravity and magnetic data from GMAF.

### Acknowledgements

The first author acknowledges the students of Geosciences Department at UAE University for their field support.

### Author contributions

HS: conceptualization, data curation, funding acquisition, resources, methodology, roles/writing—original draft. MA: investigation, software. JB: investigation, writing—review and editing. AG: resources, writing—review and editing. ARF: investigation, writing—review and editing. All authors read and approved the final manuscript.

### Funding

The first author acknowledges the financial support of UAEU by Research Start-Up Grant No. 8, Fund 31S264 (2016).

### Availability of data and materials

Data available on request from the corresponding author.

### Declarations

#### Competing interests

The authors declare that they have no known competing financial interests or personal relationships that could have appeared to influence the work reported in this paper.

Received: 20 September 2021 Accepted: 27 November 2022

Published online: 12 December 2022

### References

- Abdel ZM, Saibi H, Mansour K, Khalil A, Soliman M. Geothermal exploration using airborne gravity and magnetic data at Siwa Oasis, Western Desert, Egypt. *Renew Sustain Energy Rev*. 2018;82(3):3824–32.
- Abdel Zaher M, Elbarbary S, Sultan SA, El-Qady G, Ismail A, Takla EM. Crustal thermal structure of the Farafra oasis, Egypt, based on airborne potential field data. *Geothermics*. 2018;75:220–34. <https://doi.org/10.1016/j.geothermics.2018.05.006>.
- Abdelghany. Early Maastrichtian larger foraminifera of the Qahlah Formation, United Arab Emirates and Sultanate of Oman border region. *Cretac Res*. 2006;27(6):898–906.
- Agard P, Omrani J, Jolivet L, Whitechurch H, Vrielynck B, Spakman W, Monie P, Meyer B, Wortel R. Zagros orogeny: a subduction-dominated process. *Geol Mag*. 2011;148(5–6):692–725. <https://doi.org/10.1017/S001675681100046X>.
- Agocs WB. Least-squares residual anomaly determination. *Geophysics*. 1951;16:686–96.
- Al-Farraj A, Harvey AM. Desert pavement characteristics on wadi terrace and alluvial fan surfaces Wadi Al-Bih UAE and Oman. *Geomorphology*. 2000;35(3–4):279–97. [https://doi.org/10.1016/S0169-555X\(00\)00049-0](https://doi.org/10.1016/S0169-555X(00)00049-0).

- Ali MY, Sirat M, Small J. Integrated gravity and seismic investigation over the Jabal Hafit structure: implications for basement configuration of the frontal fold-and-thrust belt of the northern Oman mountains. *J Pet Geol*. 2009;32(1):31–7. <https://doi.org/10.1111/j.1747-5457.2009.00433.x>.
- Baranov V. A new method for interpretation of aeromagnetic maps, pseudo-gravimetric anomalies. *Geophysics*. 1957;22:359–63.
- Baranov V, Naudy H. Numerical calculation of the formula of reduction to the magnetic pole. *Geophysics*. 1964. <https://doi.org/10.1190/1.1439334>.
- Baranov V (1975) Potential fields and their transformation in applied geophysics. *Geoexploration Monographs*, series 1–6, Gebrüder, Borntraeger, Berlin—Stuttgart
- Bilim F, Aydemir A, Ates A. tectonics and thermal structure in the Gulf of Iskenderun (southern Turkey) from the aeromagnetic, borehole and seismic data. *Geothermics*. 2017;70:206–21. <https://doi.org/10.1016/j.geothermics.2017.06.016>.
- Breesch L, Swennen R, Vincent B. Fluid flow reconstruction in hanging and footwall carbonates: compartmentalization by Cenozoic reverse faulting in the Northern Oman Mountains (UAE). *Mar Petrol Geol*. 2009;26:113–28.
- Breton J-P, Béchenne F, Le Métour J, Moen-Maurel L, Razin P. Eoalpine (Cretaceous) evolution of the Oman Tethyan continental margin: insights from a structural field study in Jabal Akhdar (Oman Mountains). *GeoArabia*. 2004;9:41–58.
- Butler K. Microgravity and gravity gradient techniques for detection of subsurface cavities. *Geophysics*. 1984;49:1084–96. <https://doi.org/10.1190/1.1441723>.
- Cordell L, Grauch VJS Mapping basement magnetization zones from aeromagnetic data in the San Juan Basin, New Mexico, in *The Utility of Regional Gravity and Magnetic Anomaly Maps*. In: Hinze WJ Ed Soc Explor Geophys. 1985, 181–197. <https://doi.org/10.1190/1.0931830346.ch16>
- El-Mamhudi A, Gabr A. Two-dimensional electrical imaging of quaternary aquifer at Wadi Muraykhat and Wadi Sa'a Al-Ain Area, UAE, 7th Annual Scientific Research Conference, UAEU, Al-Ain, Conf. Proceed. 2006; 2: 278–287
- Fajkiewicz Z. The use of Cracovien computation in estimating the regional gravity. *Geophysics*. 1959;24:465–78.
- Gailler L-S, Bouchot V, Martelet G, Thion I, Coppo N, Baltassat J-M, Bourgeois B. Contribution of multi-method geophysics to the understanding of a high-temperature geothermal province: the Bouillante area (Guadeloupe, Lesser Antilles). *J Volcanol Geoth Res*. 2014;275:34–50. <https://doi.org/10.1016/j.jvolgeores.2014.02.002>.
- Glennie KW, Boeuff MGA, Hughes-Clarke MW, Moody-Stuart M, Pilaar WHF, Reinhart BM. *Geology of the Oman Mountains*. Kon Ned Geol Minnhoukundia Genoot Vern. 1974;33:423.
- Hudson RGS. The Permian and Triassic of the Oman peninsula, Arabia. *Geol Mag*. 1960;97:299–308.
- Hudson RGS, Chatton M. The Musandam Limestone (Jurassic to lower Cretaceous) of Oman Arabia. *Notes Memoirs Moyen-Orient*. 1959;3:69–93.
- Hunt TM, Bromley CJ, Risk GF, Sherburn S, Soengkono S. Geophysical investigations of the Wairakei field. *Geothermics*. 2009;38:85–97. <https://doi.org/10.1016/j.geothermics.2008.11.002>.
- Jolivet L, Faccenna C. Mediterranean extension and the Africa-Eurasia collision. *Tectonics*. 2000;19(6):1095–106. <https://doi.org/10.1029/2000TC900018>.
- Kobrunov AI. Mathematical base of theory for geophysical data interpretation. Ukta: Ukta University; 2007.
- Kobrunov AI, Varfolomeev VA. One approach of density equivalent representation and using it for gravity field interpretation. *Earth Physics USSR Acad Sci*. 1981;10:25–44.
- Komazawa M. A gravimetric terrain correction method by assuming annular prism model. *J Geod Soc Jpn*. 1988;34(1):11–23.
- Li L, Huang D, Han L, Ma G. Optimised edge detection filters in the interpretation of potential field data. *Explor Geophys*. 2014;45(2014):171–6. <https://doi.org/10.1071/EG13059>.
- Le Mouél JL. Le leve' aeromagnetique de La France, calcul des Comosantes du champ a' partir de l'intenensite. *Ann Geophysique*. 1969;26(2):229–58.
- Nettleton LI. Gravity and magnetic in oil processing. New York: McGraw Hill; 1976. p. 217–23.
- Petrel. Petrel Multiphysics Plug-in. <https://www.software.slb.com/products/petrel/petrel-geophysics/petrel-multiphysics-plugin>. 2022
- Priezzhev I, Pftzner H. US Grant 8700372B2: Method for 3-D gravity forward modeling and inversion in the wavenumber domain. 2011.
- Priezzhev I. Distribution of physical parameters according join inversion of gravity and seismic data. *Geophysica*, EAGO (Russia), 2005; 3.
- Priezzhev I. Integrated interpretation technique of geophysical data for geological modeling. Post doc thesis, State University of Sergo ordjonikidze (Moscow); 2010; 232 (in Russian Language).
- Pringle JM, Styles P, Howell CP, Branston MW, Furner R, Toon SM. Long-term time-lapse microgravity and geotechnical monitoring of relict salt mines, Marston, Cheshire, UK. *Geophysics*. 2012;77:B287–94. <https://doi.org/10.1190/geo2011-0491.1>.
- Saibi H. Various geoscientific investigations of low-enthalpy geothermal sites in the United Arab Emirates, in *Proceedings of the 43rd Workshop on Geothermal Reservoir Engineering*, Stanford University, California, USA, February 12–14, 2018; 2018.
- Saibi H, Gabr A, Baker H, Al Bloushi K. 3-D magnetic inversion at Al-Mubazzarah area, Al-Ain, United Arab Emirates, in *Proceedings of the 4th International Conference on Engineering Geophysics (ICEG)*, Al-Ain, UAE, 9–12 October 2017; 2017.
- Saibi H, Amir G, Mohamed FS. Subsurface structural mapping using gravity data of Al-Ain Region, Abu Dhabi Emirate, United Arab Emirates. *Geophys J Int*. 2019a;216:1201–13. <https://doi.org/10.1093/gji/ggy489>.
- Saibi H, Amrouche M, Fowler A, Gabr A. Magnetic density variations with depth beneath Al-Ain (UAE): implications for bed-rock structure control on hot spring waters circulation. 5th International Conference on Engineering Geophysics 2019b, 21–24 October UAEU. UAE. 2019b.
- Saibi H, Batir J, Pocasangre C. Hydrochemistry and geothermometry of thermal waters from UAE and their energetic potential assessment. *Geothermics*. 2021a;92: 102061. <https://doi.org/10.1016/j.geothermics.2021.102061>.
- Saibi H, Amrouche M, Batir J, Pocasangre C, Hussein S, Gabr A, Aldahan A, Baker H, Nishijima J, Gottsmann J (2021b) 3D geologic model and energy potential estimation of UAE geothermal systems Mubazzarah-Ain Faidha and Ain-Khatt. *Proceedings World Geothermal Congress*, 2021 +1, Reykjavik, Iceland, April – October, 2021.
- Saibi H, Mia MB, Bierre M, Alkamali M. Application of remote sensing techniques to geothermal exploration at geothermal fields in the United Arab Emirates. *Arab J Geosci*. 2021c;14:1251. <https://doi.org/10.1007/s12517-021-07633-y>.

- Saibi H, Khosravi S, Cherkose BA, Smirnov M, Kebede Y, Fowler A. Magnetotelluric data analysis using 2D inversion: a case study from Al-Mubazzarah geothermal area, Al-Ain, United Arab Emirates. *Heliyon*. 2021d;7(6): e07440. <https://doi.org/10.1016/j.heliyon.2021.e07440>.
- Searle MP. Thrust tectonics of the Dibba zone and the structural evolution of the Arabian continental margin along the Musandam Mountains (Oman and United Arab Emirates). *J Geol Soc*. 1988;145(1):43–53. <https://doi.org/10.1144/gsjgs.145.1.0043>.
- Searle M, Ali MY. Structural and tectonic evolution of the Jabal Sumeini-Al Ain–Buraimi region, northern Oman and eastern United Arab Emirates. *GeoArabia*. 2009;14(1):115–42.
- Searle MP, James NP, Calon TJ, Smewing JD. Sedimentological and structural evolution of the Arabian continental margin in Musandam Mountains and Dibba zone, United Arab Emirates. *Geol Soc Am Bull*. 1983;94(12):1381–400. [https://doi.org/10.1130/0016-7606\(1983\)94%3c1381:SAEOT%3e2.0.CO;2](https://doi.org/10.1130/0016-7606(1983)94%3c1381:SAEOT%3e2.0.CO;2).
- Sirat M, de Jong S, Werner E, Sokoutis D, Willingshofer E, Ali M. The tectonic evolution of Jebel Hafit and Al-Jaww Plain: structural style and fracture analysis. *Geophys Res Abstracts EGU*. 2007;9:01269.
- Stampfli GM, Borel GD. A plate tectonic model for the Paleozoic and Mesozoic constrained by dynamic plate boundaries and restored synthetic oceanic isochrones. *Earth Planet Sci Lett*. 2002;196(1–2):17–33. [https://doi.org/10.1016/S0012-821X\(01\)00588-X](https://doi.org/10.1016/S0012-821X(01)00588-X).
- Sudhir J. Total magnetic field reduction—the Pole or Equator? A model study. *Can J Explor Geophys*. 1988;24(1):185–92.
- Woodward D. Contributions to a shallow aquifer study by reprocessed seismic sections from petroleum exploration surveys, eastern Abu Dhabi, United Arab Emirates. *J Appl Geophys*. 1994;31(1–4):271–89. [https://doi.org/10.1016/0926-9851\(94\)90062-0](https://doi.org/10.1016/0926-9851(94)90062-0).
- Zaineldeen U, Fowler A. Structural style and fault kinematics of the Lower Eocene Rus Formation at Jabal Hafit area, Al Ain, United Arab Emirates (UAE). *Arab J Geosci*. 2014;7(3):1115–25. <https://doi.org/10.1007/s12517-013-0908-3>.

## Publisher's Note

Springer Nature remains neutral with regard to jurisdictional claims in published maps and institutional affiliations.

**Submit your manuscript to a SpringerOpen<sup>®</sup> journal and benefit from:**

- Convenient online submission
- Rigorous peer review
- Open access: articles freely available online
- High visibility within the field
- Retaining the copyright to your article

---

Submit your next manuscript at ► [springeropen.com](https://www.springeropen.com)

---